Materials for life sciences

3D-printed scaffolds for tissue engineering applications using thermosensitive hydrogels based on biopolymer blends

Ioanna Koumentakou[1], Anna Michopoulou[2,3], Michiel Jan Noordam[1], Zoi Terzopoulou[1,*] , and Dimitrios N. Bikiaris[1,*]

[1] *Laboratory of Polymer and Colors Chemistry and Technology, Department of Chemistry, Aristotle University of Thessaloniki, 54124 Thessaloniki, Greece*

[2] *Biohellenika Biotechnology Company, Thessaloniki, Greece*

[3] *Laboratory of Biological Chemistry, Medical School, Aristotle University of Thessaloniki, 54124 Thessaloniki, Greece*

ABSTRACT

Three-dimensional (3D) printing is an emerging technology for the construction of complex 3D constructs used for tissue engineering applications. In this study, we are proposing the preparation of 3D printing hydrogel inks consisting of the synthetic polymers poly(caprolactone) and poly(lactic acid), the biopolymer chitosan, and naturally derived gelatin. In addition, pluronic F-127 was used to improve the miscibility between the hydrophobic and hydrophilic components due to its amphiphilic character, as well as for its good 3D printability. The printability of the hydrogel inks was optimized by varying the composition, the extrusion nozzle, and the temperature, while the integrity of the 3D scaffolds was secured via sol–gel transition. The produced hydrogels with PCL-pluronic-chitosan-gelatin/15-20-4-2 wt% (PC3.75-Pl5-CG) and PLA-pluronic-chitosan-gelatin/10-20-4-2 wt% (PL2.5-Pl5-CG) presented the best printability, producing smooth and uniform porous scaffolds. The prepared hydrogels were formed via the interactions between the polymers through hydrogen bonding. Additionally, the produced hydrogels exhibited temperature-dependent swelling behavior, and the scaffolds with PCL presented lower swelling capacity than the scaffolds with PLA. The produced scaffolds presented slower hydrolyzation rate in simulated body fluid (SBF) at 25 °C compared to 37 °C. Biological studies proved that the 3D-printed porous scaffolds were non-cytotoxic and promoted human adipose-derived mesenchymal stem cell adhesion.
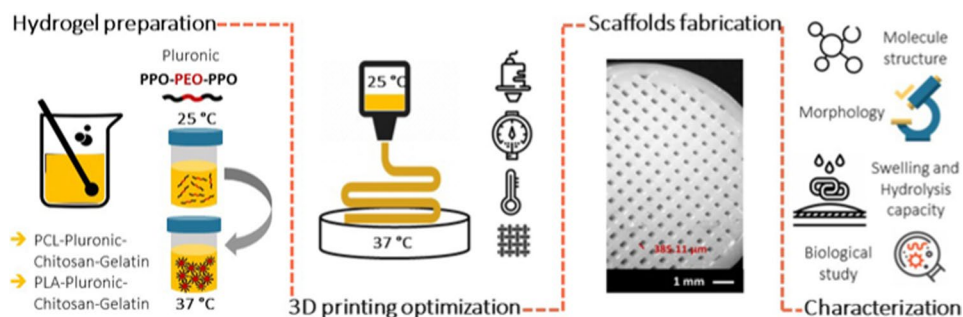
GRAPHICAL ABSTRACT

Introduction

The demand for engineered tissues has risen rapidly owing to the limited availability of donor tissues and organs for transplantation, such as bone, cartilage, skin, blood vessels, and muscle. Scaffolds are fabricated to facilitate successful tissue regeneration. These are intended to provide porous structures appropriate for cell adhesion, migration, growth, and differentiation [1]. Conventional scaffold fabrication techniques include freeze-drying, micro-/nanoimprinting, lithography, and electrospinning. However, although these methods are easy and versatile processes for the fabrication of extracellular matrix (ECM)-mimicking micro-/nanostructure or two-dimensional (2D) micro-/nanopatterns, the construction of realistic macroscale three-dimensional (3D) structures with controllable micro-/nanopatterns and uniform 3D pore geometries, including controllable and accurate porosity as well as stability, remains challenging [2]. Three-dimensional printing has seen rapid technological development over the last two decades, since it is extensively used in tissue engineering and regenerative medicine to develop complex tissue substitutes that restore the function of damaged tissues. Three-dimensional bioprinting is the layer-by-layer deposition of biomaterial hydrogels in a predetermined structural architecture to generate functional tissues or organs [1]. Extrusion-based 3D printing uses a syringe and piston system to dispense hydrogel through nozzles, which can produce stable 3D structures using highly viscous hydrogels, but it is challenging to construct structures with high mechanical stability and good printability [3]. Hydrogel requirements for 3D bioprinting of ideal engineered tissues are the following: high porosity, rapid gelation, shape retention,

and lack of immunogenicity. A variety of natural and synthetic polymers have been used for the fabrication of 3D-printed scaffolds for tissue engineering applications [4]. Poly(caprolactone) (PCL) or poly(lactic acid) (PLA) was used to fabricate 3D-printed tissue engineering scaffolds with uniformly distributed, well-formed interconnected porous structures with high bracket strength [5]. Although synthetic biodegradable polymers have good mechanical strength, thereby overcoming previous limitations on shape, size, and structural integrity, they have low biocompatibility [3]. For this reason, synthetic polymer hydrogels for 3D printing have been combined with bioactives such as nanohydroxyapatite, bioglasses [6, 7], and biological agents, as well as natural polymers like chitosan (CS) [8], collagen [9], gelatin (Gel) [10], and alginate [11] to improve the cytocompatibility, biocompatibility, biodegradability, and bioactivity of scaffolds. Among these, CS is widely used for wound healing and tissue engineering since it can promote hemostasis by clotting blood, supporting cell proliferation, and inhibiting bacterial growth [12]. Gel is a thermosensitive natural polymer that has a composition almost identical to collagen, with high biocompatibility and provides a suitable environment for cell attachment and growth [13]. However, the immiscibility among the polymers for the preparation of a hydrogel suitable for 3D printing may lead to inadequate structural integrity, mechanical stability and printability, and as a result, the damaged tissues cannot be fully regenerated [2].

In this study, we are proposing a 3D printing method supplemented with adaptable material to obtain structures with high accuracy. To achieve uniform structures on 3D-printed materials (PCL, PLA, CS, and Gel), we employed pluronic F-127 (Pl,

T_m = 56 °C) as a compatibilizer, because of its amphiphilic properties at high concentrations (> 10 wt%) [14]. Pl is a poly(ethylene oxide)-poly(propylene oxide)-poly(ethylene oxide) (PEO-PPO-PEO) tri-block copolymer. It has the ability to homogenize hydrophobic and hydrophilic polymers due to its chemical structure [15]. For this reason, Pl was used to improve the compatibility between the hydrophobic and hydrophilic polymers that were used.

Additionally, it has been studied as a potential base for thermosensitive hydrogels. It has been reported that aqueous solutions of Pl (20–30 % w/w) show thermosensitive properties and can undergo a phase transformation from low viscous transparent solution at temperature (4–5 °C) to a solid–gel when heated to body temperature (37 °C) [16]. The thermoreversible Pl hydrogels are easily extruded from 3D printers, and the 3D-printed structures maintain integrity due to its sol–gel transition, but it is quite brittle and is not suitable for long-term cell viability [3]. Specifically, Lee et al. blended Pl with synthetic polymers (PCL and PLGA) and produced 3D well-formed scaffolds with high accuracy. They also proved that 3D-printed scaffolds provided a contact guide for the cultured cells [2]. Lee et al. [17] also developed 3D multilayered scaffolds consisting of collagen and 38 wt% Pl for bone tissue engineering. They proved that over the concentration of 19 wt% Pl, the multilayered scaffolds were printed well with a uniform structure.

The aim of this work is to take advantage of the synergistic properties of synthetic and naturally derived polymers to prepare a thermosensitive hydrogel that can be used for the production of 3D-printed scaffolds for tissue regeneration. Specifically, different ratios of PCL or PLA, Pl, CS, and Gel were examined, and the optimal ratios for the best printability and uniformity factors were identified. The 3D-printed scaffolds were studied for their morphology and chemical structure as well as their in vitro biological properties.

The innovation of this study lies in the development of polymeric scaffolds with precise structure, advancing scaffold production through 3D printing for tissue regeneration, as evidenced by in vitro biological experiments. It proposes solutions for the preparation of printable inks derived from immiscible polymers, encompassing hydrophobic synthetic polymers and hydrophilic naturally derived polymers, addressing thus a current challenge in tissue engineering, which is the optimization of bioinks and scaffolds. Additionally, it introduces a safer, milder scaffold stabilization method using the sol–gel process, circumventing cytotoxic risks associated with conventional crosslinking agents [18]. This enhances scaffold biocompatibility and efficacy for tissue regeneration.

Materials and methods

Materials

PCL (M_n = 54000 g/mol) and PLA (M_n = 79000 g/mol) were synthesized using the ring-opening polymerization of ε-caprolactone and L-lactide, respectively (details in the SI). Pl was kindly donated by Pharmathen SA. CS of medium molecular weight (190000–310000 Da) and a degree of deacetylation of 75–85% was supplied by Sigma-Aldrich Co. (St. Louis, MO, USA). Gelatin from bovine skin (type B) was purchased from Serva, and dichloromethane (DCM) from Scharlab (Barcelona, Spain).

Preparation of hydrogel inks

First, Gel and CS were dissolved in 6 ml of acetic acid 2% v/v aqueous solution under magnetic stirring at 60 °C, until complete homogenization. At the same time, PCL and Pl were dissolved in 4 mL of DCM under magnetic stirring for 30 min at room temperature. Then the two solutions were mixed under mechanical stirring for 15 min at 25 °C. The composition of each polymer in the final PCL:Pl:CS:Gel (PC-Pl-CG) hydrogels and their shortnames are presented in Table 1. Similarly, PLA:Pl:CS:Gel (PL-Pl-CG) hydrogels were also prepared. Briefly, Gel and CS were dissolved in an acetic acid 2% v/v aqueous solution, while PLA and Pl were dissolved in DCM under magnetic stirring for 30 min. Then the two solutions were mixed under mechanical stirring for 15 min at 25 °C. The composition of each PL-Pl-CG hydrogel is shown in Table 1.

3D printing of constructs

The resulting hydrogels were transferred in extrusion cartridges and centrifuged at 4000 rpm for 10 min to remove air bubbles. An STL file of a mesh model scaffold was utilized for the 3D printing, while the slicing of the STL sample was performed with Slic3r software. A pneumatic extrusion-based 3D bioprinter (CELLINK® Inkredible, Gothenburg, Sweden) with

Table 1 Composition and shortnames of the PC-Pl-CG and PL-Pl-CG bioinks tested

Shortname	Composition				
	PCL (wt%)	PLA (wt%)	Pl (wt%)	CS (wt%)	Gel (wt%)
PC2.5-Pl2.5-CG	10	–	10	4	2
PC3.75-Pl2.5-CG	15	–	10	4	2
PC5-Pl2.5-CG	20	–	10	4	2
PC2.5-Pl3.75-CG	10	–	15	4	2
PC3.75-Pl3.75-CG	15	–	15	4	2
PC5-Pl3.75-CG	20	–	15	4	2
PC2.5-Pl5-CG	10	–	20	4	2
PC3.75-Pl5-CG	15	–	20	4	2
PC5-Pl5-CG	20	–	20	4	2
PL2.5-Pl2.5-CG	–	10	10	4	2
PL3.75-Pl2.5-CG	–	15	10	4	2
PL5-Pl2.5-CG	–	20	10	4	2
PL2.5-Pl3.75-CG	–	10	15	4	2
PL3.75-Pl3.75-CG	–	15	15	4	2
PL5-Pl3.75-CG	–	20	15	4	2
PL2.5-Pl5-CG	–	10	20	4	2
PL3.75-Pl5-CG	–	15	20	4	2
PL5-Pl5-CG	–	20	20	4	2

stainless steel nozzles (G20 and G22 with inner diameters of 0.6 and 0.41 mm, respectively) was used. For the printability study, cuboid mesh scaffolds with 10 mm length × 10 mm width × 1.00 mm height were designed. Different layer numbers (2, 4, 8, 12, and 14 layers) with 70% infill density and an angle of 0° were printed with 25 mm/s printing speed at 25 °C and 37 °C printing temperatures. Printing was performed on plastic Petri dishes which were maintained at 37 °C. The printability and viscosity assessments were conducted using wet samples (wet structures and hydrogel inks, respectively), whereas characterization and biological evaluations of the 3D-printed structures were carried out on dried specimens. The drying protocol for the 3D-printed scaffolds involved sequential steps: initial placement at room temperature for 48 h to facilitate gradual solvent evaporation, followed by oven drying at 40 °C for 17 h. Subsequently, the samples were left at room temperature for an additional 72 h to ensure complete elimination of residual solvents.

Printability analysis

Firstly, the printability of all hydrogels was investigated by printing one layer with square perimeter (10 mm length × 10 mm width) at two different printing temperatures (25 °C and 37 °C), using G22 (internal diameter 0.41 mm) or G20 (internal diameter 0.60 mm) nozzles with printing speed of 25 mm/s for each hydrogel. The diameter of the printed fiber was compared with the nozzle diameter (diameter of theoretical straight fiber) using optical microscopy.

The formulations which allowed the printing of fiber close to the theoretical dimensions were selected and evaluated for their printability according to four printing factors (Extrudability, Uniformity, Pore, and Integrity Factors) to find the hydrogel with the best 3D printing ability.

Extrudability

The minimum extrusion pressure required to print material at an arbitrary mass flow rate is defined as extrudability. One fiber of 10 mm in length was printed at two different printing temperatures (25 °C and 37 °C), using G20 or G22 nozzle with a printing speed of 25 mm/s for each hydrogel composition. The required pressure for the printing of fiber was noted.

Uniformity factor, U

A uniformity factor was used to determine how uniform the printed fibers are in comparison with the designed STL file. For each hydrogel sample, one fiber of 10 mm length was printed at the minimum extrusion pressure, with speed of 25 mm/s, and the diameter of the printed fiber was immediately measured with optical microscopy. The U of hydrogels was determined for wet (immediately after 3D printing process) fibers. The uniformity factor of each sample is calculated according to Eq. 1.

$$U = \frac{\text{diameter of printed fiber}}{\text{internal diameter of nozzles}} \qquad (1)$$

Pore factor, Pr

A pore factor was used to determine how well the printed pores matched the designed square pores. PC3.75-Pl5-CG and PL2.5-Pl5-CG hydrogels were used to print porous scaffolds (10 mm length × 10 mm width, infill density 70%, and two layers with angle of layers 0º), printed at the minimum air pressure and speed of 25 mm/s, using G20 and G22 extrusion nozzles at 25 °C or 37 °C. The Pr of hydrogels was determined for wet (immediately after 3D printing process) structures. The pore area of the 3D-printed structures was measured immediately after printing with optical microscopy and determined using Eq. 2.

$$Pr = \frac{\text{pore area of printed scaffold}}{\text{pore area of theoretical scaffold}} \quad (2)$$

Pore area of theoretical scaffolds is 6.76 mm^2 using G20 nozzle and 8.5 mm^2 using G22 nozzle.

Integrity factor

An integrity factor was used to determine how well the thickness of the printed scaffolds matched the intended design. PC3.75-Pl5-CG and PL2.5-Pl5-CG hydrogels were used to print scaffolds with 2, 4, 8, 12, and 14 layers at the minimum extrusion pressure and speed of approximately 25 mm/s, using G20 extrusion nozzles at 25 °C, which was selected as the suitable printing temperature. The printing process of the hydrogel inks was realized on a heated working plate at 37 °C. The pore factor of printed scaffolds after the printing of every layer is calculated according to Eq. 2. The integrity of scaffolds was determined for wet (immediately after 3D printing process) scaffolds.

The 3D printing of fibers and scaffolds was repeated three times for the printability study. Three different measurements were taken with a Jenoptik (Jena, Germany) ProgRes GRYPHAX Altair camera attached to a ZEISS (Oberkochen, Germany) SteREO Discovery V20 microscope and Gryphax image capturing software in randomly selected areas under the same magnification. Specifically, the results were quantified, and their mean values ± standard deviation are summarized after image processing with ImageJ software.

Viscosity of the selected hydrogel inks

The viscosity values were evaluated from 20 to 200 rpm using a SC4-27 spindle in a BGD 157/TS (Biuged Instruments, Guangzhou, China) rotational viscometer with temperature control.

Characterization of the printed scaffolds

PC3.75-Pl5-CG and PL2.5-Pl5-CG hydrogels were used to print porous scaffolds (10 mm length × 10 mm width, infill density 90%, and 14 layers with angle of layers 0º) in order to be characterized. The 3D printing process was accomplished at the minimum air pressure and speed of 25 mm/s, using G22 extrusion nozzle at 25 °C. The characterization of the samples was performed using 3D-printed dried structures.

Structural characterization

FTIR spectra of the prepared scaffolds were recorded with a FTIR-2000 (PerkinElmer, Dresden, Germany) with KBr disks. All spectra were recorded in the range of 4000–400 cm^{-1} with 16 scans and a resolution of 2 cm^{-1}. X-ray powder diffraction patterns were recorded using an XRD diffractometer (Rigaku Miniflex II) with a CuK radiation (0.15405 nm). The samples were scanned from 5 to 45º.

Study of swelling capacity

The swelling ratio of the prepared PC3.75-Pl5-CG and PL2.5-Pl5-CG scaffolds was measured in simulated body fluid (SBF) solution with pH = 7.4 at different temperatures (20, 25, 30, 35, and 40 °C). The SBF solution was prepared according to Kokubo and Takadama [19], Table S2. The dimensions of each 3D-printed scaffold were measured before (D_0) and after (D_t) incubation in SBF for 12 h at controlled temperature. The measurements were taken in triplicate. The excess surface SBF was wiped from the scaffolds using filter paper, and their dimensions (D_t) were measured. The swelling ratios (SR) of the tested scaffolds are calculated from the following expression (Eq. 3) [20]:

$$\text{Swelling ratio}(\%) = \frac{D_t - D_0}{D_0} * 100 \quad (3)$$

where D_t denotes the dimensions of each 3D-printed scaffold after the incubation in SBF, and D_0 denotes the initial dimensions of the scaffold.

In vitro hydrolysis

Three-dimensional-printed PC3.75-Pl5-CG and PL2.5-Pl5-CG scaffolds were incubated at pH = 7.4 in SBF at 25 and 37 °C. The samples were taken out, washed with deionized water, and weighted at predetermined time intervals (1, 5, 9, 13, 19, 25, and 30 days). The remaining mass (MR) was calculated by comparing the mass after the incubation in SBF (M_t) with the initial mass (M_0) according to the following equation [21]:

$$\text{Mass remaining}(\%) = \frac{M_t}{M_0} * 100 \tag{4}$$

Biological studies

PC3.75-Pl5-CG had the best printability, so it was selected for the fabrication of 3D-printed scaffold to perform biological studies. Specifically, a circular scaffold with 10 mm diameter, infill density 90%, and 14 layers was printed at the minimum air pressure and speed of 25 mm/s, using G22 extrusion nozzle at selected printing temperature, 37 °C (Fig. 9a). The biological studies of the PC3.75-Pl5-CG were performed using dried 3D-printed structures.

Cell cultures

The cells used for the cytocompatibility and cell adhesion experiments of the materials constructed in this study were early-passage (passage 2–3), human adipose-derived mesenchymal stem cells (hAMSCs) derived from liposuction. hAMSCs were kindly provided by BIOHELLENIKA SA (Thessaloniki, Greece). The hAMSCs were cultured in Dulbecco's modified Eagle's Medium (DMEM) (BIOWEST, Nuaillé, France) supplemented with 10% fetal bovine serum (FBS) (BIOWEST, Nuaillé, France), plated onto cell culture plates at 37 °C, 5% CO_2. The cell culture medium was replaced every other day until 70% confluency, and cell detachment for cell passage was performed using 0.05% trypsin in PBS (BIOWEST, Nuaillé, France).

Cytocompatibility

Cytocompatibility of the PC3.75-Pl5-CG scaffold was assayed by performing the MTT (3-(4,5-dimethyl-2-thiazolyl)-2,5-diphenyl-2H-tetrazolium bromide) assay as described in detail elsewhere. Briefly, equal-circle pieces (5 mm) of the materials were used. The materials were subjected to disinfection by incubation in 70% ethanol overnight, rinsed in a sterile PBS solution, and equilibrated for another 24 h in supplemented DMEM w/L-glutamine (BIOWEST, #L0104-500). In parallel, hAMSCs were seeded onto 24-well plates (CELLSTAR®, Greiner Bio-One, # 662,160) and left to grow until they reached 80% confluency. This was considered as time point zero of the experiment, and an MTT assay was performed. At that time, a piece of the PC3.75-Pl5-CG scaffold was placed on top of the cells (in contact), and the MTT assay was performed after 24 h of exposure. For the MTT method, the cells were incubated with 0.5 mL of 0.1 mg/mL MTT in DMEM complete culture medium at 37 °C in a humidified atmosphere containing 5% CO_2 for 4 h or until intra-cellular purple formazan crystals were visible under microscope. Then, the MTT was removed, and solubilizing DMSO solution was added for 30 min, until cells were lysed, and purple crystals were resolved. The supernatants were transferred to a new plate for the reading of the optical density at the spectrophotometer (PerkinElmer) at 570/630 nm. Equal numbers of hAMSCs cultured in plastic and assayed similarly were considered as positive control of proliferation.

Crystal violet cell adhesion assay

To evaluate the capacity of the PC3.75-Pl5-CG scaffold to promote cell adhesion, the crystal violet cell adhesion assay was performed. This is a colorimetric assay used to measure the attachment of cells. Briefly, equal pieces of the scaffolds were placed at the bottom of 24-well plates, and hAMSCs cells were seeded onto the surface of the materials at 50000 cells/cm^2 in DMEM culture medium. After 20 min of incubation at 37 °C, 5% CO_2, the cell culture supernatant was removed, and the remaining cells were fixed using 4% paraformaldehyde (PFA) for 10 min. Then, the fixing solution was removed, and the remaining cells were stained with 1% crystal violet for 30 min at room temperature

(RT). After the removal of crystal violet, cells were washed twice with PBS, and the plates were left to dry at RT. Finally, 100 µL of 0.5% Triton X-100 in PBS was added to dissolve the attached cells, and optical density was measured at 595 nm at the spectrophotometer (PerkinElmer). Two controls were used for this experiment. The first one included equal amount of hAMSCs cells seeded onto the plastic bottom of cell culture plates, and the second included cells seeded onto plastic coated with a widely studied adhesive peptide, the tri-amino acid sequence, arginine-glycine-aspartate (RGD) (Sigma-Aldrich, # A8052) at a concentration of 10 µg/mL. Our system was beforehand validated for the RGD-induced cell attachment capacity by performing dose–response experiment using successive increasing concentrations of RGD (data not presented here). Peptide coating was performed on the surface of the PC3.75-Pl5-CG porous scaffold as well as PC3.75-Pl5-CG non-porous scaffold in order to evaluate whether the porosity enhances cell adhesion. The PC3.75-Pl5-CG non-porous scaffold was fabricated in a similar way to the porous PC3.75-Pl5-CG scaffold with the only difference being that the infill density was 100%. For the coating, the day before the onset of the experiment and before cell seeding, 10 µg/mL of RGD in PBS was added onto the desired surfaces and left at 4 °C overnight.

Cell differentiation assay

Cells reaching sub-confluency were seeded onto the plastic surface of 12-well culture plates or onto the surface of PC3.75-Pl5-CG scaffold (pieces of equal diameters) at 50,000. Cell culture media used for the differentiation procedures were purchased: StemPro Chondrogenesis Differentiation Kit (Gibco, # A1001-01), CELL Applications Human Differentiation medium (Sigma-Aldrich, # 811D-250), and StemPro Osteogenesis Differentiation Kit (Gibco, # A10072-01). Media were changed every two days for 28 days and then stained. For every staining procedure, cells on each group were firstly fixed using 10% formaldehyde (Sigma-Aldrich) for 15 at room temperature (RT) and washed gently twice with PBS. Alizarin red staining (ARS) is a dye that binds selectively to calcium salts, and it was used to analyze the matrix mineralization in osteogenic tissue. Incubation with 60% isopropanol was performed for 5 min at RT, and fixed cells were stained for 1 h with 2% ARS (Sigma-Aldrich).

To visualize proteoglycan synthesis by chondrogenic cells, alcian blue staining was performed. Alcian blue stain was prepared at 1% in 0.1-N HCl, and staining was performed for 30 min at room temperature. The accumulation of neutral lipids in adipogenic-induced cells was assayed by using a solution of 0.5% Oil Red O and incubation at room temperature for 60 min.

Statistical analysis

All data were generated in triplicate and were analyzed with either one-way, two-way, or three-way ANOVA with Tukey multicomparison tests for post-hoc testing using IBM SPSS Statistics 27. Data are presented as mean ± SD, and $p < 0.05$ was considered to be statistically significant.

Results and discussion

Preprinting studies

Printability is a term that usually refers to the extrudability, fiber formation, porosity, and shape fidelity of biomaterial inks. While the term is not strictly defined, it is used to describe, among other things, screening processes from macroscopic and microscopic images of 3D-printed constructs with the goal of choosing printing parameters and comparing different biomaterials inks [22]. In this paper, we opted to use a simple and fast approach in order to optimize the ink composition and the printing parameters, i.e., printing pressure, nozzle diameter, and temperature by investigating the quality of the printed constructs.

Table 2 shows the qualitative results of the printing tests for the different ink compositions and shows that the PC2.5-Pl2.5-CG, PC3.75-Pl2.5-CG, PC5-Pl2.5-CG, PL2.5-Pl2.5-CG, PL3.75-Pl2.5-CG, and PL5-Pl2.5-CG hydrogels were overextruded forming a 3D-printed amorphous mass of material which makes them unsuitable for printing inks. This is due to the low concentrations of Pl (10 wt%) in the compositions leading to hydrogels with high fluidity (low viscosity) that could not mantain their shape during the 3D printing process. Although by increasing the concentrations of Pl (15 wt%), this phenomenon was reduced, and the printed fiber was quite different from the theoretical. However, the dimensions of the square perimeter, which were printed using hydrogels with a high

Table 2 Printing quality of inks with different nozzle diameters and temperatures

Shortname	25 °C		37 °C	
	Nozzle gauge			
	G22	G20	G22	G20
PC2.5-Pl2.5-CG	×	×	×	×
PC3.75-Pl2.5-CG	×	×	×	×
PC5-Pl2.5-CG	×	×	×	×
PC2.5-Pl3.75-CG	~	~	~	~
PC3.75-Pl3.75-CG	~	~	~	~
PC5-Pl3.75-CG	~	~	~	~
PC2.5-Pl5-CG	✓	✓	✓	✓
PC3.75-Pl5-CG	✓	✓	✓	✓
PC5-Pl5-CG	✓	✓	✓	✓
PL2.5-Pl2.5-CG	×	×	×	×
PL3.75-Pl2.5-CG	×	×	×	×
PL5-Pl2.5-CG	×	×	×	×
PL2.5-Pl3.75-CG	~	~	~	~
PL3.75-Pl3.75-CG	~	~	~	~
PL5-Pl3.75-CG	~	~	~	~
PL2.5-Pl5-CG	✓	✓	✓	✓
PL3.75-Pl5-CG	✓	✓	✓	✓
PL5-Pl5-CG	✓	✓	✓	✓

✓: good printing quality, ~: medium printing quality (heterogeneous struts), and ×: cannot be extruded

amount of Pl (20 wt%), were close to the theoretical dimensions (Fig. 1).

Viscosity of the selected hydrogel inks

The hydrogels with 20 wt% of Pl (PC2.5-Pl5-CG, PC3.75-Pl5-CG, PC5-Pl5-CG, PL2.5-Pl5-CG, PL3.75-Pl5-CG, and PL5-Pl5-CG) were selected for further printability and viscosity evaluation.

The rheological properties of a hydrogel determine its ability to be 3D-printed and allow it to outflow through a small nozzle head [23]. For extrusion-based bioprinters, bioinks with viscosities from 300 to 30000 mPa·s are preferred. Hydrogels with a viscosity lower than 300 mPa·s are more suitable for smearing instead of printing. When the viscosity is higher than 30000 mPa·s, high pressure is required to extrude the bioink out of the nozzle, and what is more, the extrusion process will become unstable [24]. In the present work, it was found that the viscosities of the thermosensitive hydrogels were determined by two factors: their composition, and

mainly by the ratio of PCL:Pl or PLA:Pl, since their combined concentration was higher than CS and Gel, and the temperature at which they were extruded (Fig. 2).

As expected, the viscosity increased with increasing either the PCL or PLA contents in the PC-Pl-CG and PL-Pl-CG hydrogels. The PLA-containing hydrogels had larger viscosity than the PCL-containing ones [25]. This is due to the fact that the PLA used had a higher M_n and $[\eta]$ than PCL. More specifically, PCL had $M_n = 54000$ g/mol and $[\eta] = 1.23$ dL/g, while PLA had $M_n = 79000$ g/mol and $[\eta] = 1.51$ dL/g (Table S1). Additionally, by raising the temperature from 25 to 37 °C, the viscosity of the hydrogels increased due to the presence of Pl, as it undergoes a phase transition from liquid to gel at 37 °C [26]. The sol–gel transition while increasing the temperature is attributed to the micellization phenomenon. Pl has a central hydrophobic PPO block and two hydrophilic PEO on both sides. The hydrophobic PPO block dehydrates increasing the temperature from 25 to 37 °C as a result of the formation of spherical micelles. The formatted micelles are made of a dehydrated PPO core and an outer shell of hydrated swollen PEO chains. This micellization is followed by the gelation process, leading to concentrated gels. As a result, the prepared hydrogels with high Pl concentration (20 wt%) had slightly lower viscosity at room temperature (25 °C) than at body temperature (37 °C), where a gel was formed [27]. This small difference in viscosity strongly affects the printability of the hydrogels as discussed below. This is confirmed by the literature, where it was reported that formulations with 15–30 wt% concentration of Pl are liquid at room temperature, whereas transforming into a gel form at body temperature [28]. However, in this work, PC-Pl-CG and PL-Pl-CG hydrogels could not be liquid at room temperature due to the presence of CS and Gel polymers which act co-operatively in hydrogel formation, specifically the macromolecules of CS form gels when in acidic media due to the electrostatic repulsions of its positively charged amino groups. Additionally, the negatively charged groups of the Gel macromolecules in the solutions interact with the positively charged amino groups of CS, forming a viscous hydrogel [29]. The viscosity assessment results suggest that all PC-Pl-CG and PL-Pl-CG hydrogels are suitable for printing complex 3D structures.

Figure 1 Stereoscope images of fiber produced with 3D printing using hydrogels with different Pl concentrations while keeping the concentrations of PCL (15 wt%), PLA (10 wt%) CS (4 wt%), and Gel (2 wt%) stable.
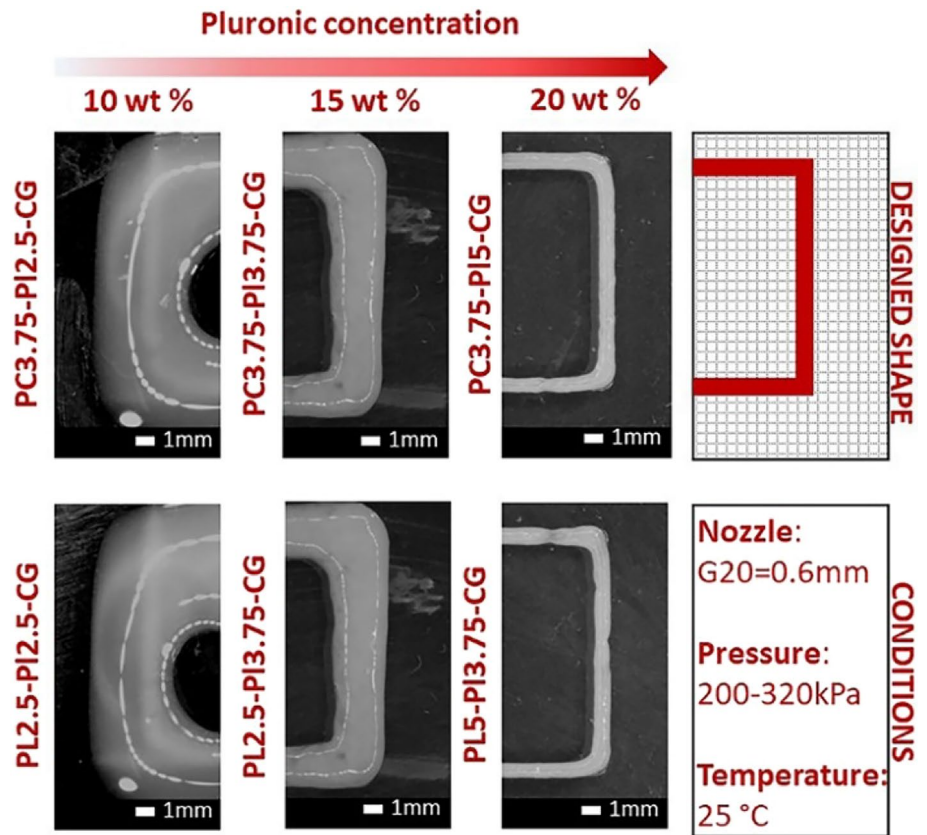
Printability studies

After the measurement of the viscosity, the printability of the PC2.5-Pl5-CG, PC3.75-Pl5-CG, PC5-Pl5-CG, PL2.5-Pl5-CG, PL3.75-Pl3.75-CG, and PL5-Pl3.75-CG hydrogels were investigated, and specifically, the extrudability, uniformity, pore, and integrity factors were calculated.

First, the necessary pressure to achieve extrudability was determined. Extrudability is the capability to extrude bioink through a nozzle to form a continuous and controllable fiber. Table 3 shows the minimum air pressure required for the extrusion of the studied hydrogels. Table 3 and Fig. 3 show that the required air pressure (P) for extrusion was affected by the viscosity of the hydrogels. Specifically, the decrease in either PCL or PLA concentrations or temperature (from 37 to 25 °C) reduced the required air pressure, which was expected since the viscosity was also smaller [30]. For example, PC2.5-Pl5-CG hydrogel (10 wt% PCL content) required 185 kPa to be extruded at 25 °C, while PC5-Pl5-CG with increased PCL content (20 wt%) at 25 °C required 300 kPa (using the G22 nozzle in both cases). Additionally, PC5-Pl5-CG required 244 kPa

to be extruded at 25 °C while higher pressure was needed, 289 kPa at 37 °C. Furthermore, the PL-Pl-CG hydrogels require higher air pressure to be extruded (230–378 kPa) than PC-Pl-CG (169–344 kPa) hydrogels which is consistent with the viscosity results as PL-Pl-CG presented higher viscosity (Fig. 3). Nozzle size also affected the P, since a decrease in the diameter of the nozzle size from 0.60 mm (G20) to 0.41 mm (G22) resulted in an increase in the P (Fig. 3) [24].

The viscosity of the thermosensitive hydrogels also affects the printing accuracy of the structures. The printing accuracy of the selected hydrogels was investigated by calculating the fiber uniformity factor (U), and the results are illustrated in Fig. 4. The hydrogels with low viscosity expanded after the extrusion, causing the lateral collapse of the printed material and the deformation of the printed fiber, with $U > 1$. On the other hand, the highly viscous hydrogels could not be extruded smoothly from the small needle, and as a result, the fibers did not spread ($U < 1$) (Fig. 4c) [31, 32].

The hydrogel composition significantly affected the U. Multiple comparisons resulted in $p < 0.005$ between all compositions except for PC5-Pl5-CG vs.
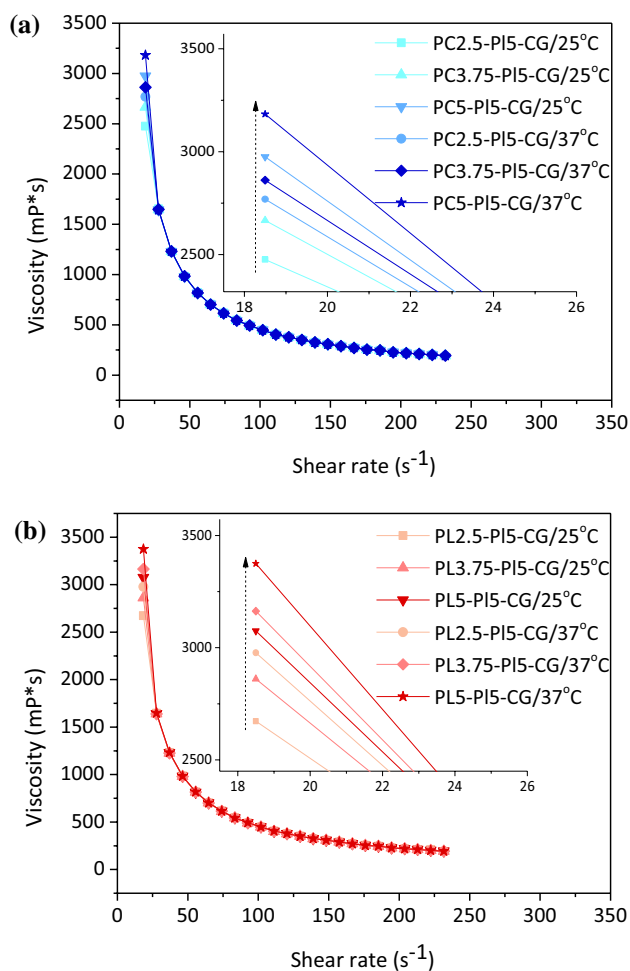
Figure 2 Viscosity test of **a** PC-Pl-CG and **b** PL-Pl-CG hydrogels at 25 °C and 37 °C.

PL3.75-Pl5-CG which was insignificant ($p > 0.05$). PC2.5-Pl5-CG had the lowest viscosity of all hydrogels and a $U = 1.5$, while PC5-Pl5-CG with the highest viscosity had $U = 0.6$ when using G20 nozzle at 25 °C (Fig. 4a). Overall, PC3.75-Pl5-CG and PL2.5-Pl5-CG had the best 3D printing results, as their Us were the closest to the theoretical value ($U = 1$). Specifically, PC3.75-Pl5-CG and PL2.5-Pl5-CG had $U = 1.018$ and 0.966 with G20 nozzle and $U = 0.9911$ and 0.941 using G22, respectively (at 25 °C), producing continuous fibers (Fig. 4a) [17]. As shown in Fig. 4, the reduction in nozzle diameter size caused a significant decrease in U ($p < 0.005$) due to the difficulty of the hydrogels to flow throughout the smaller nozzle (G22). Moreover, the increase in the temperature (from 25 to 37 °C) had an overall effect on U ($p < 0.005$) as it increased the hydrogel's viscosity which does not allow the homogenous extrusion and thus the uniform printing of the hydrogel, leading to uncompleted structures (Fig. 4d). For example, PL2.5-Pl5-CG presented $U = 0.94$ at 25 °C with G22 (Fig. 4a), proving that the printed fiber was very close to the theoretical fiber ($U = 1$). On the other hand, PL2.5-Pl5-CG printed dotted fiber at 37 °C (Fig. 4b) with G22, presenting U considerably less than unity ($U = 0.63$) due to its increased viscosity.

Pr of PC3.75-Pl5-CG and PL2.5-Pl5-CG hydrogels, which had the best U of all studied hydrogels, was evaluated and confirmed that the hydrogel inks presented significantly better printability at 25 °C than 37 °C ($p < 0.005$). The pores structures that were printed at 37 °C had irregular-shaped pores instead of square pores, due to a non-continuous flow of the material through the nozzle, resulting in a relatively

Table 3 The minimum air pressure required for the extrusion of all hydrogels

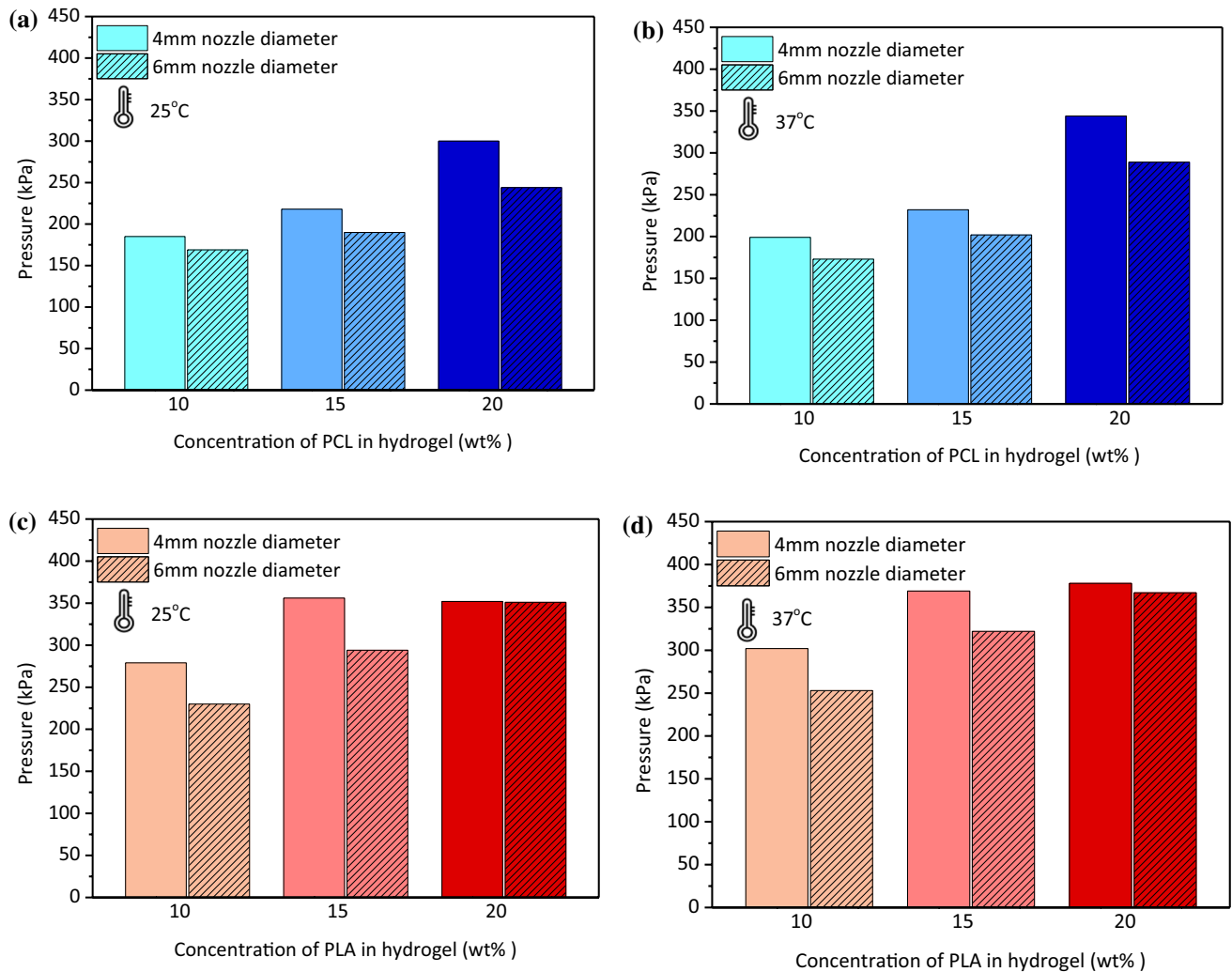| Hydrogel	Nozzle size	Air pressure (kPa) required for extrusion at 25 °C	Air pressure (kPa) required for extrusion at 37 °C
PC2.5-Pl5-CG	G22	185	199
	G20	169	173
PC3.75-Pl5-CG	G22	218	232
	G20	190	202
PC5-Pl5-CG	G22	300	344
	G20	244	289
PL2.5-Pl5-CG	G22	279	302
	G20	230	253
PL3.75-Pl5-CG	G22	356	369
	G20	294	322
PL5-Pl5-CG	G22	352	378
	G20	351	367

Figure 3 The effect of PCL (**a** and **b**) and PLA (**c** and **d**) concentration as well as the diameter of nozzle size on the applied pressure during the printing process.

high mean Pr (Fig. 5). In contrast, the pores printed at 25 °C had square shapes and better reproducibility (Pr values being nearly the optimum value of 1), independently of the nozzle size. Specifically, PC3.75-Pl5-CG had perfect pore printability and accuracy, with Pr = 1.031 at 25 °C, while the pore factor was 1.226 at 37 °C, using G22 nozzle size (Fig. 5a and b). The viscosity increase at 37 °C is attributed to the high content of Pl in hydrogels and results in the low penetration of the inks through the nozzle. Despite the better Pr values obtained with G20, the statistical effect of nozzle diameter is insignificant, likely due to small sample size. Although PL2.5-Pl5-CG had a good uniformity factor, the pore factor showed a higher deviation than the theoretical (Pr = 1), being Pr = 1.06 and Pr = 1.21 at

25 °C and 37 °C, respectively, when using G22 nozzle (Fig. 5a), but the difference is still statistically insignificant ($p > 0.05$) proving that the quality between the two compositions is negligible. The high M_n value of PLA resulted in the formation of a compact hydrogel that exhibited an excellent printing ability for short, simple arrangements, such as fiber structures, but a poorer performance for complex structures with fabricating requirements, such as pore scaffolds. Pore size, shape accuracy, and integrity are critical parameters that define a scaffold's performance. At an early stage, tissue regeneration happens at the periphery of scaffolds with a negative gradient in mineralization toward the inner structure. For cell adhesion, continuous ingrowth of tissue, and synthesis of uniform
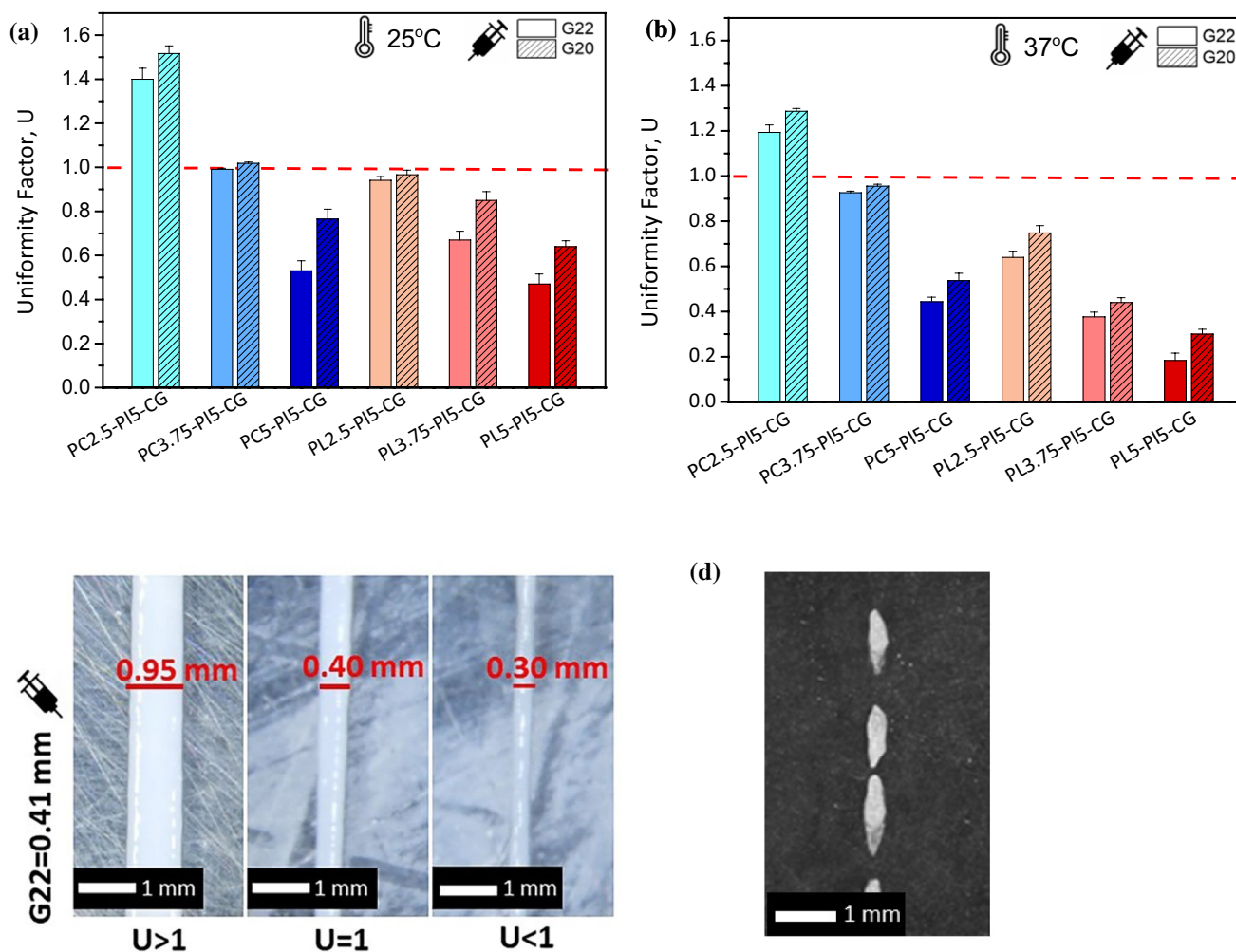
Figure 4 The investigation of uniformity factor of the thermo-sensitive hydrogels at **a** 25 °C and **b** 37 °C. Three-way ANOVA showed a significant effect of temperature, hydrogel sample type, and nozzle diameter on the uniformity factor ($p < 0.005$). **c** Sche-matic illustration of the uniformity factor of the hydrogels: a non-uniform fiber with $U \neq 1$ and a uniform fiber with $U = 1$. **d** Uncompleted fiber structure with $U \neq 1$.

tissue, the interconnected porosity with high shape accuracy is necessary [33].

Thus, based on the results, 25 °C was selected as the appropriate temperature in the extrusion cartridge to successfully achieve a smooth and uniform well-formed mesh structure.

The printing process of the thermosensitive hydrogels was realized on a heated working plate at 37 °C to ensure the integrity of the printed pore structures due to the sol–gel nature of Pl. Figure 6 illustrates the Pr values of the printed mesh with different numbers of layers, using PC3.75-Pl5-CG and PL2.5-Pl5-CG hydrogels at 25 °C with G20. The shape of PC3.75-Pl5-CG was retained regardless of the number of layers. Increasing the layers from 2 to 4 did not cause a

significant difference in Pr; rather than further increasing it caused a reduction in Pr, but still within acceptable values close to 1. This is due to the fact that Pl-based hydrogel inks give thermoresponsive structures which are well-formed and stable at 37 °C, avoiding the radial diffusion of the layers toward the center of the structure. On the other hand, PL2.5-Pl5-CG presented diffusion and fusion phenomena during the printing of a 14-layer structure. The printed pores narrowed radially, and the sidewalls of the printed structures presented layer misalignment and deformation during printing (Fig. 6) [24]. This might be due to the lower amount of PLA (10 wt%) that was used in comparison with PC0.75-PlC0.2G0.1 which contained 15 wt% PCL, and as a result, more inconstant
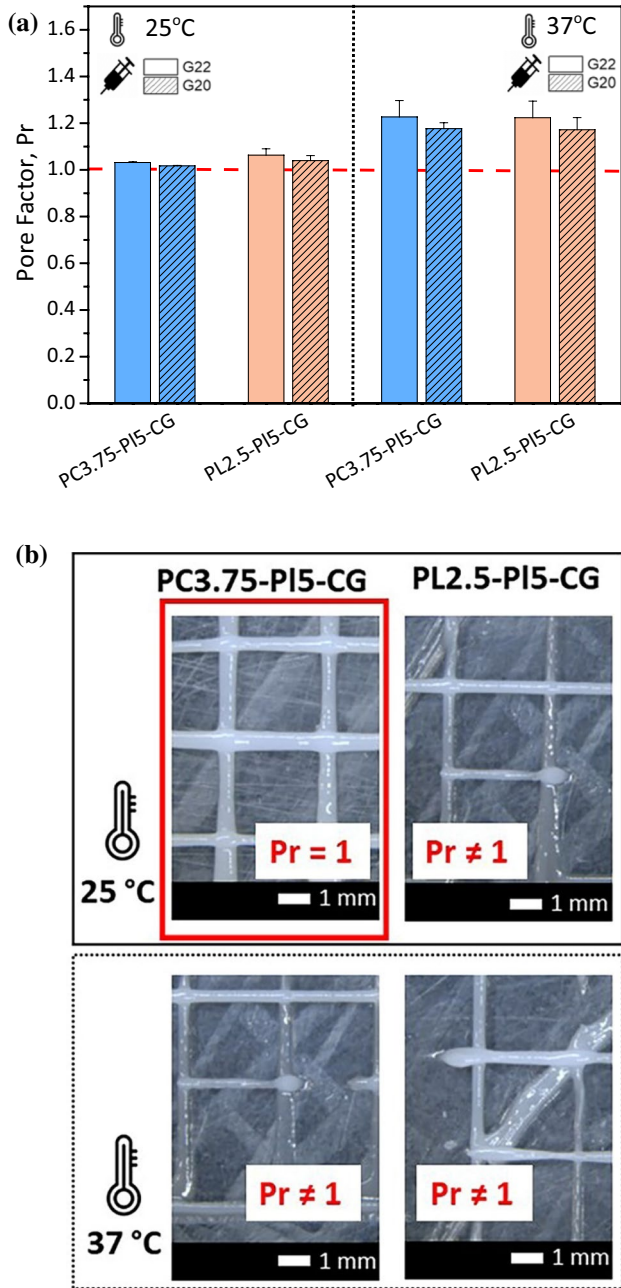
Figure 5 **a** Pore factor of the hydrogels printed at 25 °C and 37 °C. Three-way ANOVA showed a significant effect of temperature on the uniformity factor ($p < 0.005$). **b** Optical microscopy images used to determine the pore factor: a non-uniform pore with $Pr \neq 1$ and a uniform pore with $Pr = 1$.
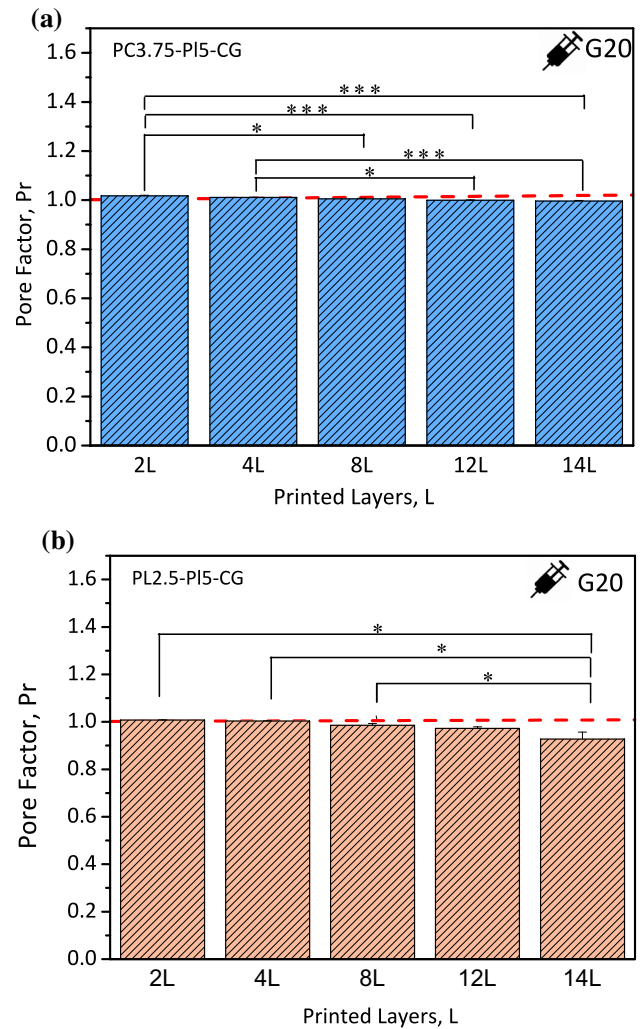

Figure 6 Pore factor of the **a** PC3.75-Pl5-CG and **b** PL2.5-Pl5-CG printed porous structures with different layers. One-way ANOVA, $*p < 0.005$.

precision at 25 °C due to their liquid–hydrogel form, and the 14-layer printed mesh model showed good shape retention at 37 °C, avoiding the use of photoinitiators or chemical crosslinking agents that may cause toxic effects [17]. The PL2.5-Pl5-CG hydrogel showed similar thermosensitive behavior as PC3.75-Pl5-CG but lower printability and printing accuracy.

Structural characterization

In Fig. 7a, the FTIR spectra of Pl, PCL, PLA, CS, and Gel are presented. The spectrum of Pl is characterized by the CH_2 stretching vibrations around 2878 cm^{-1} and C–O–C stretching signals in the 1008 cm^{-1} [31].
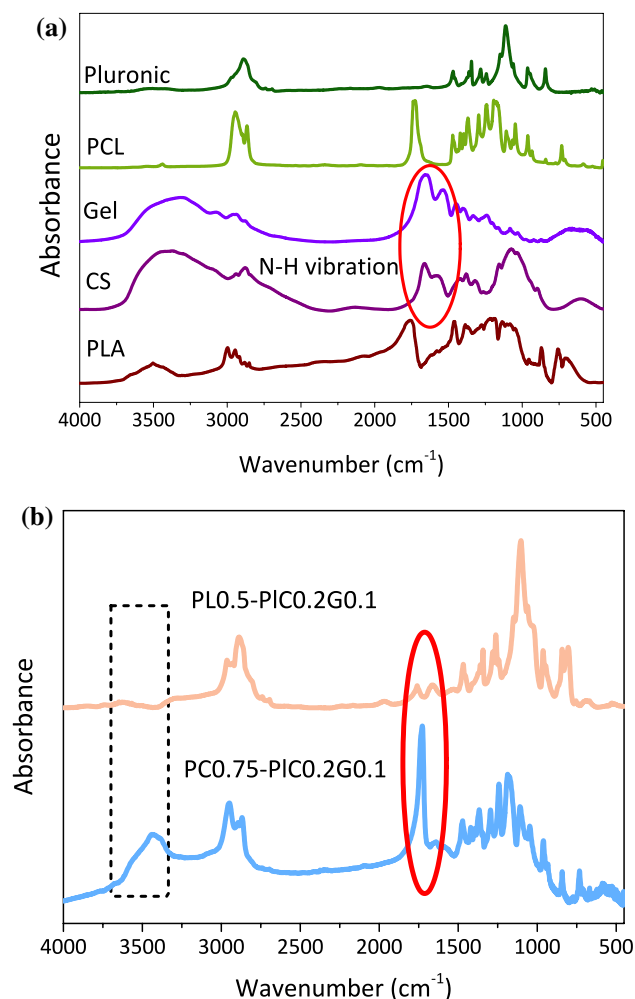
structures were formed. This was reflected by the statistically significant reduction of Pr when increasing the layers from 2, 4, or 8 to 14.

Hence, it was concluded that multiple layers of PC3.75-Pl5-CG hydrogel can be printed with high

Figure 7 FTIR spectra of **a** Pl, PCL, PLA, CS, and Gel and **b** 3D-printed scaffolds PC3.75-Pl5-CG and PL2.5-Pl5-CG.

Figure 8 XRD pattern of **a** PCL, PLA, CS, Gel, and PI **b** 3D-printed scaffolds PC3.75-Pl5-CG and PL2.5-Pl5-CG.

The spectrum of PCL shows the characteristic peaks of CH_2 (2943 and 2862 cm^{-1}) and C=O stretching vibrations (1720 cm^{-1}). The C–O and C–C stretchings are centered at 1296 cm^{-1}, while symmetric and asymmetric C–O–C stretchings at 1247 and 1190 cm^{-1}, respectively. PLA shows characteristic stretching frequencies for C=O, –CH$_3$ asymmetric, –CH$_3$ symmetric, and C–O, at 1759, 2999, 2949, and 1080 cm^{-1}, respectively. Bending frequencies for –CH$_3$ asymmetric and –CH$_3$ symmetric have been identified at 1455 and 1381 cm^{-1}, respectively [34]. Additionally, the typical bands of the CS polysaccharide structure are present at 3326 cm^{-1}, due to the O–H vibrations, at 1643 cm^{-1} (amide I), 1565 cm^{-1} (NH$_2$ bending), and 1378 cm^{-1} (CH$_2$ bending) [35]. The characteristic absorption bands of Gel in the spectra are situated at 1233 cm^{-1} due to C–N and N–H vibrations in amide III, whereas

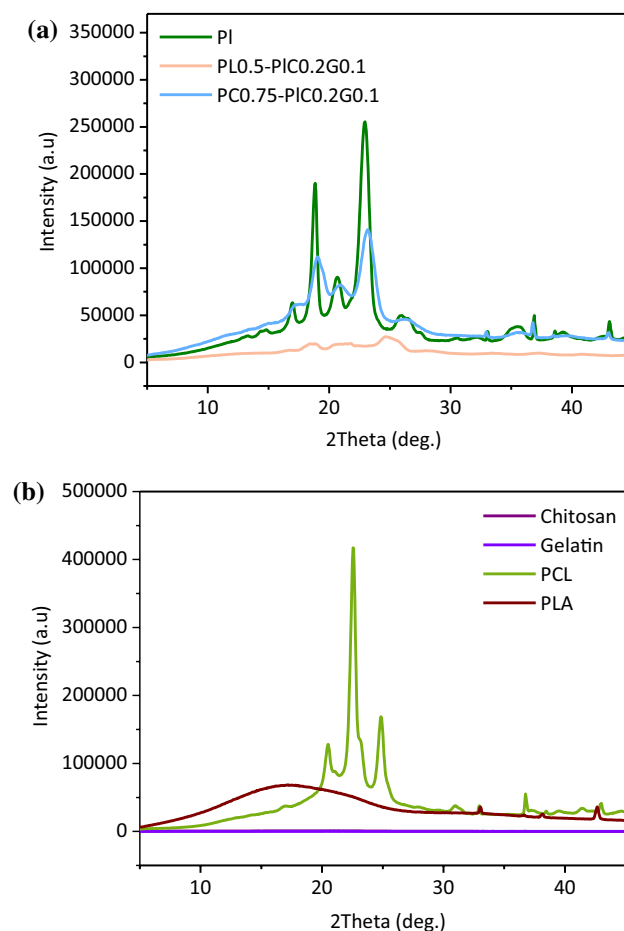1533 cm^{-1}, 3302 cm^{-1}, and 1663 cm^{-1} are the peaks corresponding to C–N and N–H vibrations in amide II, to O–H stretching vibration and C=O and N–H vibrations in amide I, respectively [36]. The spectra of the PC3.75-Pl5-CG and PL2.5-Pl5-CG (Fig. 7b) exhibit the characteristic peaks of all polymers and the shift of two characteristic bands which correspond to O–H stretching vibration and N–H vibrations, confirming the interactions of the polymers through hydrogen bonding between the amino and hydroxyl moieties [37].

The XRD patterns of Pl, PCL, PLA, CS, and Gel as well as PC3.75-Pl5-CG and PL2.5-Pl5-CG scaffolds are illustrated in Fig. 8. The presence of the sharp peaks at 18.8° and 23° is characteristic of the structure of Pl, with crystalline domains embedded within the amorphous regions [38]. The diffraction pattern of the crystalline PCL reveals the presence of crystallinity with peaks at $2\theta = 22.5°$ and 24.7° corresponding to the

(110) and (200) crystal planes [39]. PLA showed only a broad diffraction peak centered at $2\theta \approx 16.8°$, indicating its semi-crystalline structure [40]. The XRD patterns of CS and Gel confirmed the amorphous structure of these polymers [41]. PC3.75-Pl5-CG printed structures exhibited only the characteristic peaks of Pl with low intensity, while the PL2.5-Pl5-CG scaffold did not have any crystalline peaks (Fig. 8b). The reduction of the intensity and the disappearance of some peaks indicate a decrease in the degree of crystallinity

(a)

(b)

Figure 9 **a** Swelling capacity of PC3.75-Pl5-CG and PL2.5-CG scaffolds at different temperatures at pH = 7.4. One-way ANOVA showed insignificant effect of hydrogel composition ($p > 0.05$). Significant differences were detected with changing the temperature, *$p < 0.005$. **b** MR of PC3.75-Pl5-CG and PL2.5-Pl5-CG scaffolds at 25 °C and 37 °C at pH = 7.4. One-way ANOVA with repeated measurements showed a significant overall effect of temperature on MR.

of the scaffold due to the interactions among the polymers [42].

Study of swelling and hydrolysis capacity

Figure 9a shows the swelling ratios of 3D-printed PC3.75-Pl5-CG and PL2.5-Pl5-CG scaffolds. The results showed that PC3.75-Pl5-CG and PL2.5-Pl5-CG do not behave different from one another. More specifically, PC3.75-Pl5-CG showed a swelling capacity of 234% at 30 °C, and PL2.5-Pl5-CG presented similar percentages of 251%. Additionally, the 3D-printed PC3.75-Pl5-CG and PL2.5-Pl5-CG scaffolds showed similar temperature sensitivities due to the high amount of Pl (20 wt%) that they contained. The swelling ratio of the scaffolds continuously decreased with increasing temperature, and a significant effect of temperature was observed when increasing it from 20 °C or 25 °C to either 35 °C or 40 °C and from 30 to 40 °C. However, there is no significant difference of swelling between the groups measured at 35 °C and at 30 °C as $p > 0.05$. The deswelling behavior of the scaffolds was due to the micellization of the Pl component, which was induced by raising the temperature. Pl tri-block copolymers crosslinked CS inter- and intra-molecularly, and the thermally induced Pl micellization restricted the swelling tendency of CS chains [43]. The crosslinking of the hydrogel reduced the mesh size of the scaffolds at higher temperatures, thereby decreasing the overall swelling ratio.

The temperature also affected the MR of PC3.75-Pl5-CG and PL2.5-Pl5-CG scaffolds due to the hydrolysis of the ester linkage of Pl (Fig. 9). Both types of hydrogels had a significantly faster degradation rate compared to 37 °C than 25 °C, even though they were less hydrated with increasing temperature. At 37 °C, the remaining mass of the PC3.75-Pl5-CG and PL2.5-Pl5-CG scaffolds was 54% and 43% after 30 days, respectively. In contrast, at 25 °C, no extensive degradation occurred since the mass loss of the prepared scaffolds was less than 30% during the incubation period of 30 days. This occurred due to the thermally induced formation of Pl micelle domains in the hydrogel that is likely to contract a CS chain network. Therefore, increased junction tension between the Pl and CS chains decreased the swelling capacity of the scaffolds and allowed the ester linkage to be cleaved more readily, leading to the structure's hydrolysis [43].

Additionally, the hydrolysis of PL2.5-Pl5-CG was faster than PC3.75-Pl5-CG. In particular, the RM of
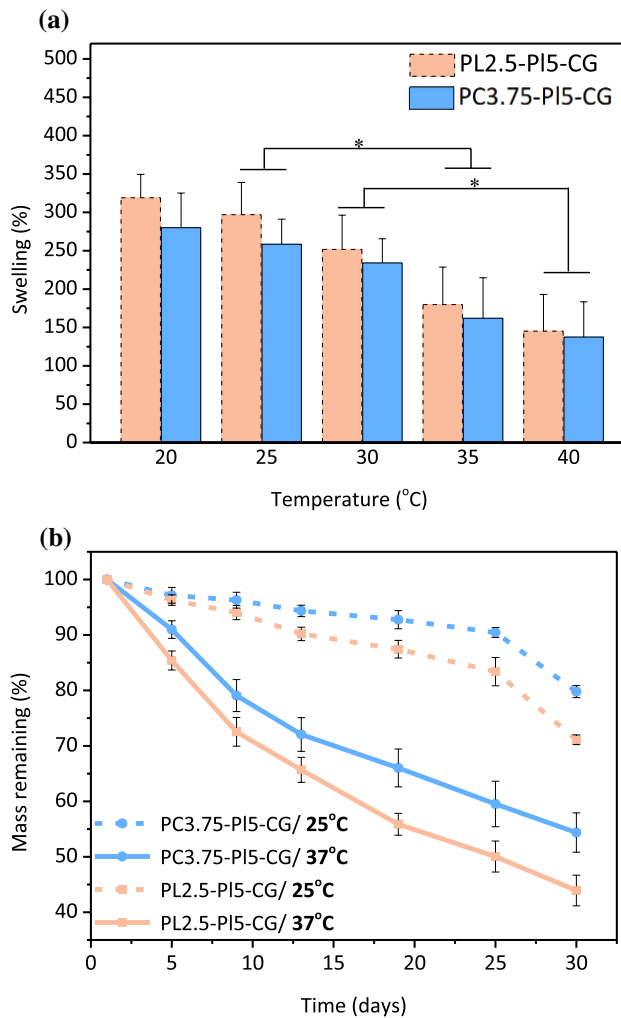
PL2.5-Pl5-CG was 71% and 43% at 25 °C and 37 °C, respectively, while the RM of PC3.75-Pl5-CG was 79% and 54% at 25 °C and 37 °C, respectively, after 30 days. This might be due to easier penetration of water molecules in the PL2.5-Pl5-CG hydrogel network, causing more extensive and faster hydrolysis. This is also supported by the swelling studies where more water molecules penetrated the polymer matrix of the PL2.5-Pl5-CG scaffold than the PC3.75-Pl5-CG scaffold due to the lower content of hydrophobic polymer in PL2.5-Pl5-CG (10 wt% PLA) than PC3.75-Pl5-CG (15 wt% PCL) [44].

In the literature, it was shown that a scaffold should have a hydrolysis time of 25 days to be suitable for skin regeneration applications, proving that PC3.75-Pl5-CG and PL2.5-Pl5-CG could be appropriate for skin tissue regeneration [45].

In vitro cell studies

A scaffold must have a suitable pore size with high pore accuracy for continuous ingrowth of tissue [46].

Open and interconnected pores allow nutrients and molecules to diffuse within the inner parts of a scaffold to facilitate cell growth, vascularization, as well as waste material removal. An ideal scaffold for inducing skin regeneration should possess a suitable microstructure with a pore size of 100–200 mm and > 90% porosity [47]. However, Ewa Dzierzkowska et al. proved that PLA porous scaffolds with pore size of 40–400 µm facilitated high keratinocytes viability [48]. In the present work, porous scaffolds with pore size of 380–400 µm were manufactured, and their biological properties were evaluated (Fig. 10a).

Since all materials utilized as scaffolds must have low cytotoxicity, it was critical to investigate the toxicity/compatibility of the newly synthesized 3D-printed scaffolds [49, 50]. For this reason, the possible cytotoxic effect of the new scaffolds on hAMSCs cells after 24 h of exposure was evaluated via the MTT assay. MTT can be used as a tool for the relative estimation of cell growth rate. The addition of a material to a cell culture can have a temporary impact on cell growth, and cells may need time to adjust to the new culture

Figure 10 **a** Three-dimensional-printed PC3.75-Pl5-CG porous scaffolds used for biological studies. **b** Cytotoxicity/cytocompatibility of the PC3.75-Pl5-CG printed scaffold. The cell proliferation rate after 24 h of exposure estimated via MTT analysis. Comparisons were made by measuring optical densities at the time 0 and 24 h after exposure to the materials or culture onto plastic. **c** Adhesive properties of the printed materials. One-way ANOVA ($\#p < 0.05$, $*p < 0.005$).
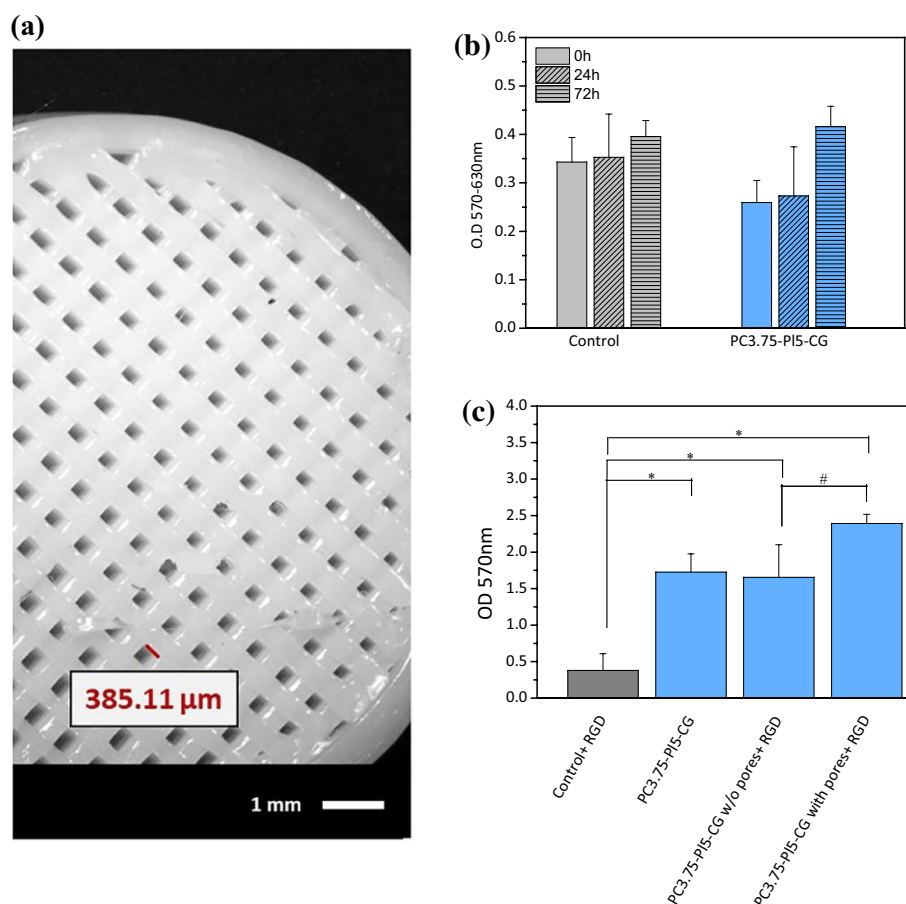
condition. In order to avoid false responses due to experimental artifacts, cell growth was measured at two time points per condition, one soon after adding the materials into the cell cultures (time point 0) and one at 24 h of exposure. According to the obtained results (Fig. 10b, c), no significant difference between control and the samples was observed, with a small decreasing trend in OD, but the % cell viability on PC3.75-Pl5-CG scaffold is ~ 75%, which is within the acceptable range for non-cytotoxicity. No significant difference was found between the timepoints 0 h and 24 h either. Thus, the cell viability on the scaffold was comparable to that of the control. Nevertheless, after 72 h, a notable increase in cell count was observed, indicating the potential of the scaffold to serve as a substrate for cell proliferation and tissue regeneration.

The capacity of a material to support cell adhesion is a rather critical property for promoting tissue development at the sites of implantation and also for the delivery of reparative cells at wound sites for the materials that serve as cell-carriers [51]. In order to evaluate the capacity of PC3.75-Pl5-CG scaffold to support cell attachment, the crystal violet cell adhesion assay was performed [52]. The PC3.75-Pl5-CG scaffold appeared to have excellent adhesive properties since cell adhesion to the scaffold was significantly greater as compared to the plastic surface of the cell culture plate. Having obtained this important result and in order to confirm and further evaluate the adhesive capacity of the scaffold, a comparison was also performed after coating the plastic surface of the culture plate with a widely studied adhesive peptide, the tri-amino acid sequence, arginine-glycine-aspartate (RGD). Interestingly, cell adhesion onto the surface of the PC3.75-Pl5-CG scaffolds was significantly higher than on the RGD adhesive peptide. Interactions between the cell surface and the cytoskeleton appears to play an important role in the regulation of cell function through the production of signals transmitted via the integrins to the cytoskeleton. Through the procedure of cell adhesion, the cells can "sense" their surrounding environment and respond to biochemical and mechanical changes [53]. Several glycoproteins are known to be involved in the binding of cells to the extracellular matrix (ECM), such as collagen, fibronectin, and laminin. Some of the adhesion-promoting ECM proteins contain specific peptide sequences such as RGD through which they bind to transmembrane receptors named integrins [54]. Based on the observations mentioned above several groups have tried to incorporate or coat RGD onto new materials intended for tissue engineering purposes [55]. To that end, a coating was performed onto two types of the PC3.75-Pl5-CG scaffolds with and without pores, and the cells adhesion properties were re-evaluated. Our preliminary results demonstrated that coating the scaffolds with the RGD peptide further enhanced the cell adhesion capacity suggesting a biological relevance. These data, on one hand, provided solid proof of the PC3.75-Pl5-CG scaffolds with porous structure adhesive properties and, on the other hand, constituted preliminary evidence of the benefits of functionalizing this scaffold with RGD in the future for tissue engineering applications.

Finally, preliminary experiments were performed with the aim to assess the maintenance of the well-documented capacity of hASCs for tri-lineage differentiation, when they are cultured onto the PC3.75-Pl5-CG scaffolds (Fig. 11). The obtained data confirmed the latter notion, suggesting that the PC3.75-Pl5-CG scaffolds possess a number of properties that collectively will allow their use for tissue engineering applications in the future.

Conclusions

In this work, new hydrogel inks consisting of synthetic (PCL and PLA) and naturally derived Gel and CS polymers were prepared. Furthermore, Pl was utilized to mix the hydrophobic and hydrophilic polymers, due to its amphiphilic character, as well as for its good printability. Specifically, PCL-Pl-CS-Gel and PLA-Pl-CS-Gel hydrogels were prepared with nine different compositions. The printability of the hydrogels was investigated by changing the extrusion nozzle size (G20 and G22) and temperature (25 °C and 37 °C), and it was found that PCL-Pl-chitosan-gelatin/15-20-4-2%wt (PC3.75-Pl5-CG) and PLA-Pl-CS-Gel/ 10-20-4-2%wt (PL2.5-Pl5-CG) had the best printability, yielding uniform scaffolds. However, it was proved that the sol–gel nature of Pl played a decisive role in the printing process, as hydrogels were printed with high precision at 25 °C due to their liquid–hydrogel form, but the printed mesh model showed good shape retention at 37 °C due to their gel form. FTIR analysis showed interactions among the hydrogel's components through hydrogen bonding. In addition, the hydrogels exhibited temperature-dependent swelling and hydrolysis behaviors in aqueous media, which was presumably caused by the local micellization of the
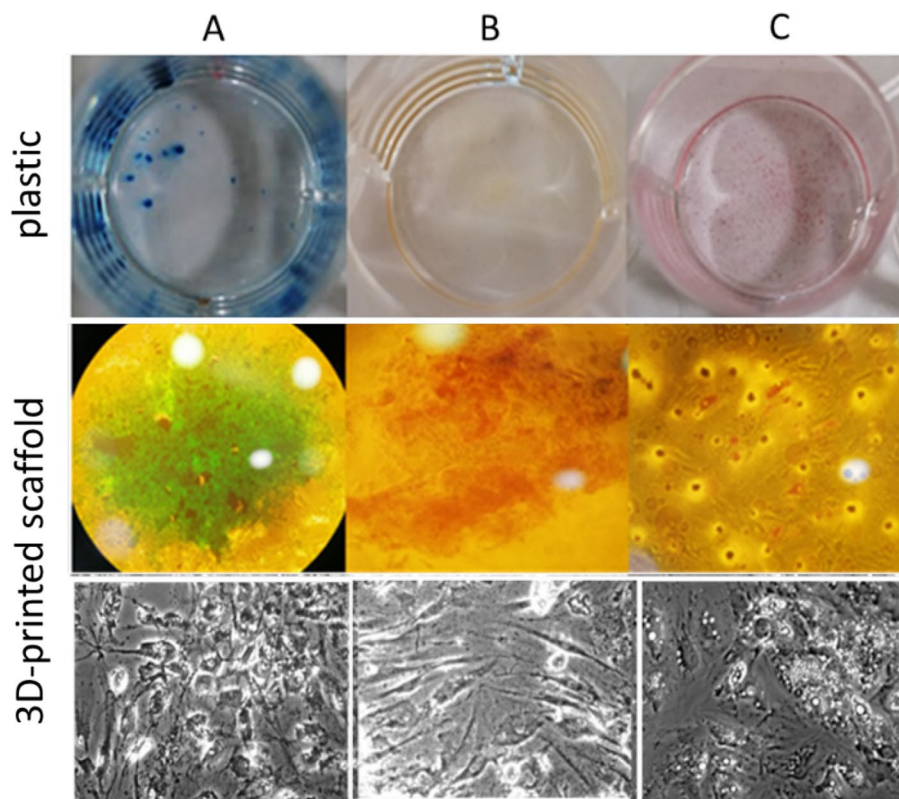
Figure 11 Differentiation capacity of hAMSCs cultured in 3D conditions using the PC3.75-Pl5-CG scaffold. Column **A**, presents induced differentiation capacity of hASCs to chondrocytes, column **B** represents osteogenesis, and column **C** represents adipogenesis, using a standard differentiation protocol. hASCs cultured onto plastic were used as a control of the induction and compared to cells cultured onto the scaffold. The first and second rows show confirmation of the differentiation of hASCs cells by staining, and the third row by cells' morphology in light microscopy images (scale bar 50 μm). Differentiation was confirmed using specialized staining procedure for each tissue type, ie., alcian blue, alizarin red, and Oil Red O, respectively.

Pl with increasing temperature. The swelling capacity decreased as well, and mass loss occurred much faster at a higher temperature. In vitro cell studies proved that the prepared 3D-printed porous scaffolds were non-cytotoxic and promoted cell adhesion and differentiation. Such thermoresponsive and degradable Pl hydrogels can be potentially used for tissue engineering applications.

Author contributions

Ioanna Koumentakou was involved in writing—original draft, methodology, investigation, formal analysis, and data curation. Michiel Jan Noordam was involved in formal analysis, data curation, and conceptualization. Anna Michopoulou was involved in investigation, analysis, and writing—original draft. Zoi Terzopoulou contributed with writing—review and editing, supervision, and conceptualization. Dimitrios N. Bikiaris helped with conceptualization, writing—review and editing, supervision, and resources.

Declarations

Conflict of interest The authors declare that they have no known competing financial interests or personal relationships that could have appeared to influence the work reported in this paper.

Ethical approval There are no ethical issues involved in this study.

Supplementary Information The online version contains supplementary material available at https://doi.org/10.1007/s10853-024-09707-0.

References

[1] Lazaridou M, Bikiaris DN, Lamprou DA (2022) 3D bioprinted chitosan-based hydrogel scaffolds in tissue engineering and localised drug delivery. Pharmaceutics 14:1978. https://doi.org/10.3390/pharmaceutics14091978

[2] Lee JU, Chae SJ, Lee H, Kim GH (2020) A 3D printing strategy for fabricating in situ topographical scaffolds using pluronic F-127. Addit Manuf 32:101023. https://doi.org/10.1016/j.addma.2019.101023

[3] Kang H-W, Lee SJ, Ko IK, Kengla C, Yoo JJ, Atala A (2016) A 3D bioprinting system to produce human-scale tissue constructs with structural integrity. Nat Biotechnol 34:312–319. https://doi.org/10.1038/nbt.3413

[4] Ligon SC, Liska R, Stampfl J, Gurr M, Mülhaupt R (2017) Polymers for 3D printing and customized additive manufacturing. Chem Rev 1517:10212–10290. https://doi.org/10.1021/acs.chemrev.7b00074

[5] Jiao Z, Luo B, Xiang S, Ma H, Yu Y, Yang W (2019) 3D printing of HA / PCL composite tissue engineering scaffolds. Adv Ind Eng Polym Res 2:196–202. https://doi.org/10.1016/j.aiepr.2019.09.003

[6] Terzopoulou Z, Baciu D, Gounari E, Steriotis T, Charalambopoulou G, Tzetzis D, Bikiaris D (2019) Composite membranes of poly(ϵ-caprolactone) with bisphosphonate-loaded bioactive glasses for potential bone tissue engineering applications. Molecules 24:3067. https://doi.org/10.3390/molecules24173067

[7] Solechan S, Suprihanto A, Widyanto SA, Triyono J, Fitriyana DF, Siregar JP, Cionita T (2023) Characterization of PLA/PCL/nano-hydroxyapatite (nHA) biocomposites prepared via cold isostatic pressing. Polymers (Basel) 15:559. https://doi.org/10.3390/polym15030559

[8] Haaparanta AM, Järvinen E, Cengiz IF, Ellä V, Kokkonen HT, Kiviranta I, Kellomäki M (2014) Preparation and characterization of collagen/PLA, chitosan/PLA, and collagen/chitosan/PLA hybrid scaffolds for cartilage tissue engineering. J Mater Sci Mater Med 25:1129–1136. https://doi.org/10.1007/s10856-013-5129-5

[9] Zhou DS, Zhao KB, Li Y, Cui FZ, Lee IS (2006) Repair of segmental defects with nano-hydroxyapatite/collagen/PLA composite combined with mesenchymal stem cells. J Bioact Compat Polym 21:373–384. https://doi.org/10.1177/0883911506068554

[10] Yu F, Li M, Yuan Z, Rao F, Fang X, Jiang B, Wen Y, Zhang P (2018) Mechanism research on a bioactive resveratrol–PLA–gelatin porous nano-scaffold in promoting the repair of cartilage defect. Int J Nanomedicine 13:7845–7858. https://doi.org/10.2147/IJN.S181855

[11] Kundu J, Shim JH, Jang J, Kim SW, Cho DW (2015) An additive manufacturing-based PCL-alginate-chondrocyte bioprinted scaffold for cartilage tissue engineering. J Tissue Eng Regen Med 9:1286–1297. https://doi.org/10.1002/term.1682

[12] Bergonzi C, Di Natale A, Zimetti F, Marchi C, Bianchera A, Bernini F, Silvestri M, Bettini R, Elviri L (2019) Study of 3D-printed chitosan scaffold features after different post-printing gelation processes. Sci Rep 9:1–11. https://doi.org/10.1038/s41598-018-36613-8

[13] Meng Y, Cao J, Chen Y, Yu Y, Ye L (2020) 3D printing of a poly(vinyl alcohol)-based nano-composite hydrogel as an artificial cartilage replacement and the improvement mechanism of printing accuracy. J Mater Chem B 8:677–690. https://doi.org/10.1039/c9tb02278c

[14] Russo E, Villa C (2019) Poloxamer hydrogels for biomedical applications. Pharmaceutics 11:671. https://doi.org/10.3390/pharmaceutics11120671

[15] Guo Q, Liu C, Hai B, Ma T, Zhang W, Tan J, Fu X, Wang H, Xu Y, Song C (2018) Chitosan conduits filled with simvastatin/pluronic F-127 hydrogel promote peripheral nerve regeneration in rats. J Biomed Mater Res–Part B Appl Biomater 106:787–799. https://doi.org/10.1002/jbm.b.33890

[16] Kaisang L, Siyu W, Lijun F, Daoyan P, Xian CJ, Jie S (2017) Adipose-derived stem cells seeded in pluronic F-127 hydrogel promotes diabetic wound healing. J Surg Res 217:63–74. https://doi.org/10.1016/j.jss.2017.04.032

[17] Lee J, Kim G (2018) Three-dimensional hierarchical nanofibrous collagen scaffold fabricated using fibrillated collagen and pluronic F-127 for regenerating bone tissue. ACS Appl Mater Interfaces 10:35801–35811. https://doi.org/10.1021/acsami.8b14088

[18] Akbuǧa J, Durmaz G (1994) Preparation and evaluation of cross-linked chitosan microspheres containing furosemide. Int J Pharm 111:217–222. https://doi.org/10.1016/0378-5173(94)90344-1

[19] Takadama TKÃH (2006) How useful is SBF in predicting in vivo bone bioactivity. Biomaterials 27:2907–2915. https://doi.org/10.1016/j.biomaterials.2006.01.017

[20] Im O, Li J, Wang M, Zhang LG, Keidar M (2012) Biomimetic three-dimensional nanocrystalline hydroxyapatite and magnetically synthesized single-walled carbon nanotube chitosan nanocomposite for bone regeneration. Int J Nanomedicine 7:2087–2099. https://doi.org/10.2147/IJN.S29743

[21] Xu H, Yang X, Xie L, Hakkarainen M (2016) Conformational footprint in hydrolysis-induced nanofibrillation and crystallization of poly(lactic acid). Biomacromol 17:985–995. https://doi.org/10.1021/acs.biomac.5b01636

[22] Schwab A, Levato R, Este MD, Piluso S, Eglin D, Malda J (2020) Printability and shape fidelity of bioinks in 3D bioprinting. Chem Rev 120:11028–11055. https://doi.org/10.1021/acs.chemrev.0c00084

[23] Chen H, Wang P, Zheng C, Zhang L (2022) Thermal-responsive and 3D printable hydrogel based on an acylhydrazine-terminated dynamic covalent bond and pluronic F127. ACS Appl Polym Mater 4:6312–6321. https://doi.org/10.1021/acsapm.2c00410

[24] He Y, Yang F, Zhao H, Gao Q, Xia B, Fu J (2016) Research on the printability of hydrogels in 3D bioprinting. Sci Rep 6:29977. https://doi.org/10.1038/srep29977

[25] Jun Z, Hou H, Schaper A, Wendorff JH, Greiner A (2003) Poly-L-lactide nanofibers by electrospinning–influence of solution viscosity and electrical conductivity on fiber diameter and fiber morphology. E-Polymers 3:009. https://doi.org/10.1515/epoly.2003.3.1.102

[26] Park KM, Lee SY, Joung YK, Na JS, Lee MC, Park KD (2009) Thermosensitive chitosan-pluronic hydrogel as an injectable cell delivery carrier for cartilage regeneration. Acta Biomater 5:1956–1965. https://doi.org/10.1016/j.actbio.2009.01.040

[27] Müller M, Becher J, Schnabelrauch M, Zenobi-Wong M (2015) Nanostructured pluronic hydrogels as bioinks for 3D bioprinting. Biofabrication 7:35006. https://doi.org/10.1088/1758-5090/7/3/035006

[28] Chen Y, Lee JH, Meng M, Cui N, Dai CY, Jia Q, Lee ES, Jiang HB (2021) An overview on thermosensitive oral gel based on poloxamer 407. Materials (Basel) 14:4522. https://doi.org/10.3390/ma14164522

[29] Voron'ko NG, Derkach SR, Kuchina YA, Sokolan NI (2016) The chitosan-gelatin (bio)polyelectrolyte complexes formation in an acidic medium. Carbohydr Polym 138:265–272. https://doi.org/10.1016/j.carbpol.2015.11.059

[30] Lin S, Li B, Yang L, Zhai Y, Wang X, Wang C (2022) New method for reducing viscosity and shear stress in hydrogel 3D printing via multidimension vibration. Comput Methods Biomech Biomed Engin 25:1796–1811. https://doi.org/10.1080/10255842.2022.2039129

[31] Spadola G, Sanna V, Bartoli J, Carcelli M, Pelosi G, Bisceglie F, Restivo FM, Degola F, Rogolino D (2020) Thiosemicarbazone nano-formulation for the control of *Aspergillus* flavus. Environ Sci Pollut Res 27:20125–20135. https://doi.org/10.1007/s11356-020-08532-7

[32] Afonso JA, Alves JL, Caldas G, Gouveia BP, Santana L, Belinha J (2021) Influence of 3D printing process parameters on the mechanical properties and mass of PLA parts and predictive models. Rapid Prototyp J 27:487–495. https://doi.org/10.1108/RPJ-03-2020-0043

[33] Seitz H, Rieder W, Irsen S, Leukers B, Tille C (2005) Three-dimensional printing of porous ceramic scaffolds for bone tissue engineering. J Biomed Mater Res - Part B Appl Biomater 74:782–788. https://doi.org/10.1002/jbm.b.30291

[34] Chieng BW, Ibrahim NA, Wan Yunus WMZ, Hussein MZ (2014) Effects of graphene nanopletelets on poly(lactic acid)/poly(ethylene glycol) polymer nanocomposites. Adv Mater Res 1024:139–139. https://doi.org/10.4028/www.scientific.net/AMR.1024.136

[35] Koumentakou I, Terzopoulou Z, Michopoulou A, Kalafatakis I, Theodorakis K, Tzetzis D, Bikiaris D (2020) Chitosan dressings containing inorganic additives and levofloxacin

as potential wound care products with enhanced hemostatic properties. Int J Biol Macromol 162:693–703. https://doi.org/10.1016/j.ijbiomac.2020.06.187

[36] Chao SC, Wang MJ, Pai NS, Yen SK (2015) Preparation and characterization of gelatin-hydroxyapatite composite microspheres for hard tissue repair. Mater Sci Eng C 57:113–122. https://doi.org/10.1016/j.msec.2015.07.047

[37] Fan L, Yang H, Yang J, Peng M, Hu J (2016) Preparation and characterization of chitosan/gelatin/PVA hydrogel for wound dressings. Carbohydr Polym 146:427–434. https://doi.org/10.1016/j.carbpol.2016.03.002

[38] Medarević DP, Kachrimanis K, Mitrić M, Djuriš J, Djurić Z, Ibrić S (2016) Dissolution rate enhancement and physicochemical characterization of carbamazepine-poloxamer solid dispersions. Pharm Dev Technol 21:268–276. https://doi.org/10.3109/10837450.2014.996899

[39] Balu R, Sampath Kumar TS, Ramalingam M, Ramakrishna S (2011) Electrospun polycaprolactone/Poly(1,4-butylene adipate-co-polycaprolactam) blends: potential biodegradable scaffold for bone tissue regeneration. J Biomater Tissue Eng 1:30–39. https://doi.org/10.1166/jbt.2011.1004

[40] Zorah M, Mustapa IR, Daud N, Nahida JH, Sudin NAS, Majhool AA, Mahmoudi E (2020) Improvement thermomechanical properties of polylactic acid via titania nanofillers reinforcement. J Adv Res Fluid Mech Therm Sci 70:97–111. https://doi.org/10.37934/ARFMTS.70.1.97111

[41] Llanos JHR, Vercik LCDO, Vercik A (2015) Physical properties of chitosan films obtained after neutralization of polycation by slow drip method. J Biomater Nanobiotechnol 06:276–291. https://doi.org/10.4236/jbnb.2015.64026

[42] Gautam S, Chou CF, Dinda AK, Potdar PD, Mishra NC (2014) Fabrication and characterization of PCL/gelatin/chitosan ternary nanofibrous composite scaffold for tissue engineering applications. J Mater Sci 49:1076–1089. https://doi.org/10.1007/s10853-013-7785-8

[43] Kim MR, Park TG (2002) Temperature-responsive and degradable hyaluronic acid/Pluronic composite hydrogels for controlled release of human growth hormone. J Control Release 80:1–3. https://doi.org/10.1016/S0168-3659(01)00557-0

[44] Pavoni JMF, Luchese CL, Tessaro IC (2019) Impact of acid type for chitosan dissolution on the characteristics and biodegradability of cornstarch/chitosan based films. Int J Biol Macromol 138:693–703. https://doi.org/10.1016/j.ijbiomac.2019.07.089

[45] Terzopoulou Z, Zamboulis A, Koumentakou I, Michailidou G, Noordam MJ, Bikiaris DN (2022) Biocompatible synthetic polymers for tissue engineering purposes. Biomacromol 23:1841–1863. https://doi.org/10.1021/acs.biomac.2c00047

[46] Bose S, Vahabzadeh S, Bandyopadhyay A (2013) Bone tissue engineering using 3D printing. Mater Today 16:496–504. https://doi.org/10.1016/j.mattod.2013.11.017

[47] Jones AC, Arns CH, Sheppard AP, Hutmacher DW, Milthorpe BK, Knackstedt MA (2007) Assessment of bone ingrowth into porous biomaterials using MICRO-CT. Biomaterials 28:2491–2504. https://doi.org/10.1016/j.biomaterials.2007.01.046

[48] Dzierzkowska E, Scisłowska-Czarnecka A, Kudzin M, Boguń M, Szatkowski P, Gajek M, Kornaus K, Chadzinska M, Stodolak-Zych E (2021) Effects of process parameters on structure and properties of melt-blown poly(Lactic acid) nonwovens for skin regeneration. J Funct Biomater 12:16. https://doi.org/10.3390/jfb12010016

[49] Nakiou EA, Lazaridou M, Pouroutzidou GK, Michopoulou A, Tsamesidis I, Liverani L, Arango-ospina M, Beketova A, Boccaccini AR, Kontonasaki E, Bikiaris DN (2022) Poly (glycerol succinate) as coating material for 1393 bioactive glass porous scaffolds for tissue engineering applications. Polymers 14:5028. https://doi.org/10.3390/polym14225028

[50] Michopoulou A, Koliakou E, Terzopoulou Z, Rousselle P, Palamidi A, Doxakis A, Konstantinidou P, Roig-Rosello E, Demiri E, Bikiaris D (2022) Benefit of coupling heparin to crosslinked collagen I/III scaffolds for human dermal fibroblast subpopulations' tissue growth. J Biomed Mater Res Part A 110:797–811. https://doi.org/10.1002/jbm.a.37329

[51] Bacakova L, Filova E, Parizek M, Ruml T, Svorcik V (2011) Modulation of cell adhesion, proliferation and differentiation on materials designed for body implants. Biotechnol Adv 29:739–767. https://doi.org/10.1016/j.biotechadv.2011.06.004

[52] Humphries MJ (1998) Cell-substrate adhesion assays. Curr Protoc Cell Biol. https://doi.org/10.1002/0471143030.cb0901s00

[53] Berrier AL, Yamada KM (2007) Cell–matrix adhesion. J Cell Physiol 213:565–573. https://doi.org/10.1002/jcp.21237

[54] Arnaout MA, Mahalingam B, Xiong J-P (2005) Integrin structure, allostery, and bidirectional signaling. Annu Rev Cell Dev Biol 21:381–410. https://doi.org/10.1146/annurev.cellbio.21.090704.151217

[55] Le Guillou-Buffello D, Bareille R, Gindre M, Sewing A, Laugier P, Amédée J (2008) Additive effect of RGD coating to functionalized titanium surfaces on human osteoprogenitor cell adhesion and spreading. Tissue Eng Part A 14:1445–1455. https://doi.org/10.1089/ten.tea.2007.0292

Publisher's Note Springer Nature remains neutral with regard to jurisdictional claims in published maps and institutional affiliations.